Stem Cell Research 15 (2015) 715–721

Contents lists available at ScienceDirect

Stem Cell Research

journal homepage: www.elsevier.com/locate/scr

Short report

Highly proliferative primitive fetal liver hematopoietic stem cells are fueled by oxidative metabolic pathways

Javed K. Manesia [a,b], Zhuofei Xu [a,b], Dorien Broekaert [a,b], Ruben Boon [a,b], Alex van Vliet [c], Guy Eelen [d,e], Thomas Vanwelden [a,b], Steve Stegen [h], Nick Van Gastel [h], Alberto Pascual-Montano [f], Sarah-Maria Fendt [g], Geert Carmeliet [h], Peter Carmeliet [d,e], Satish Khurana [a,b,*,1,2], Catherine M. Verfaillie [a,b,*,2]

[a] Inter-departmental Stem Cell Institute, KU Leuven, Leuven, Belgium
[b] Department of Development and Regeneration, Stem Cell Biology and Embryology, KU Leuven, Leuven, Belgium
[c] Laboratory of Cell Death Research and Therapy, KU Leuven, Leuven, Belgium
[d] Laboratory of Angiogenesis and Neurovascular Link, KU Leuven, Leuven, Belgium
[e] Laboratory of Angiogenesis and Neurovascular Link, Leuven, Belgium
[f] Functional Bioinformatics Group, National Center for Biotechnology-CSIC, Madrid, Spain
[g] Laboratory of Cellular Metabolism and Metabolic Regulation, KU Leuven, Leuven, Belgium
[h] Clinical and Experimental Endocrinology, KU Leuven, Leuven, Belgium

ARTICLE INFO

Article history:
Received 10 July 2015
Received in revised form 16 October 2015
Accepted 2 November 2015
Available online 9 November 2015

Keywords:
Hematopoietic stem cells
Fetal liver
Bone marrow
Metabolism
Oxidative phosphorylation
Self-renewal

ABSTRACT

Hematopoietic stem cells (HSCs) in the fetal liver (FL) unlike adult bone marrow (BM) proliferate extensively, posing different metabolic demands. However, metabolic pathways responsible for the production of energy and cellular building blocks in FL HSCs have not been described. Here, we report that FL HSCs use oxygen dependent energy generating pathways significantly more than their BM counterparts. RNA-Seq analysis of E14.5 FL versus BM derived HSCs identified increased expression levels of genes involved in oxidative phosphorylation (OxPhos) and the citric acid cycle (TCA). We demonstrated that FL HSCs contain more mitochondria than BM HSCs, which resulted in increased levels of oxygen consumption and reactive oxygen species (ROS) production. Higher levels of DNA repair and antioxidant pathway gene expression may prevent ROS-mediated (geno)toxicity in FL HSCs. Thus, we here for the first time highlight the underestimated importance of oxygen dependent pathways for generating energy and building blocks in FL HSCs.

1. Introduction

In adult mammals, HSCs give rise to all the blood cells throughout life. During development, HSCs originate in the dorsal aorta, from where they migrate into the FL at E11. The FL is the main site of hematopoiesis until near birth. Around birth, HSCs migrate from the FL to the BM, where they reside during postnatal life. In the FL, HSCs undergo multiple rounds of symmetrical self-renewing cell divisions to give rise to the pool of stem cells required for the lifetime of the organisms. However, in adults, the most primitive HSCs (termed long-term repopulating (LT)-HSCs, that repopulate the hematopoietic system long-term following transplantations, are quiescent, dividing only every 140–180 days in mouse; Wilson et al. 2008; Foudi et al. 2009). BM HSC divisions are asymmetrical generating one HSC and one committed progenitor/short-term repopulating (ST)-HSC (Takano et al. 2004). Nevertheless, quiescent LTR-HSCs can respond very rapidly to stress or damage, and quickly exit from quiescence to regenerate the blood system (Cheng et al. 2000). However, this is associated with aging of LT-HSCs, demonstrated by shortening of telomeres and skewing of LT-HSC differentiation towards the myeloid lineage (Vaziri et al. 1994; Sudo et al. 2000).

Aside from phenotypic differences, functional differences have also been described between adult BM and FL LT-HSCs (Higuchi et al. 2003; Bowie et al. 2007). For instance, FL LT-HSCs display significantly faster expansion kinetics when grafted in adult mice, compared with LT-HSCs from BM of 8-week-old mice (Bowie et al. 2007). Furthermore, FL and early postnatal BM LT-HSCs undergo significantly more symmetrical self-renewing cell divisions compared with 8-week-old adult BM LT-HSCs.

Although it would be logical to hypothesize that extensively proliferating FL LT-HSCs may require a significantly different metabolic activity to create energy and building blocks for cell renewal, few if any studies have addressed this question. Cell metabolism consists of anabolic and catabolic reactions that allow cells to survive, function and synthesize

* Corresponding authors at: Stem cell Institute, KU Leuven, O&N4, Bus 804, Herestraat 49, 3000 Leuven, Belgium.
E-mail addresses: svkanand@gmail.com, satishkhurana@iisertvm.ac.in (S. Khurana), Catherine.verfaillie@med.kuleuven.be (C.M. Verfaillie).
[1] Present address: School of Biology, Indian Institute of Science Education and Research, Thiruvananthapuram, Kerala, India.
[2] These authors contributed equally as last author.

http://dx.doi.org/10.1016/j.scr.2015.11.001

new components for cellular division. The generation of cellular energy (ATP), reduction capacity (NADH, NADPH and FADH2) and cellular macromolecules is mainly fueled by the consumption of glucose, glutamine and fatty acids through glycolysis, glutaminolysis and β-oxidation, respectively (Berg et al. 2007; Matés et al. 2009). The function and activity of ATP-generating pathways is known to differ dramatically in stem cells and differentiated progeny. Most stem cells have been shown to use glycolysis for energy production, while more differentiated cells divert glucose to the mitochondria and exhibit a significantly higher rate of OxPhos (Varum et al. 2011; Abu Dawud et al. 2012). This has also been shown for adult BM LT-HSCs. Postnatal BM LT-HSCs depend on glycolysis for energy production, whereas glycolysis decreases upon differentiation and OxPhos increases (Suda et al. 2011; Klimmeck et al. 2012). While TCA cycle-related metabolites such as 2-oxoglutarate, acetyl-CoA, and succinyl-CoA were not detected in LT-HSCs, they were shown to accumulate pyruvate (Takubo et al. 2013). Loss of pyruvate dehydrogenase kinase (*Pdk*) (Takubo et al. 2013) or lactate dehydrogenase (*Ldha*) (Wang et al. 2014), which inhibits glycolysis, results in defects in LT-HSC function. As metabolic pathways used can determine fate changes at the stem cell level (Oburoglu et al. 2014), we believe that understanding the metabolism of proliferative FL LT-HSCs will provide insights into how it might be possible to achieve extensive self-renewal of BM LT-HSCs, and hence, create efficient ex vivo LT-HSC expansion systems.

In this study, we tested the hypothesis that in contrast to adult BM LT-HSCs, which use glycolysis for energy production, FL HSCs may use alternative metabolic pathways to fuel their ability to expand extensively, such as the OxPhos pathway. This hypothesis was based on results of an RNA-sequencing (RNA-seq) study we performed on E14.5 FL and 8-week-old murine LT-HSCs, to gain insight into the molecular differences between fetal and adult HSCs that underlie their functional attributes. In this screen, we surprisingly found that that FL HSCs express significantly higher levels of OxPhos and citric acid cycle (TCA) genes compared with BM HSCs.

2. Materials and methods

2.1. Animals

Six to 10 weeks old C57BL/6J-CD45.2 mice (Centre d'Elevage R. Janvier, Le Genest-St. Isle, France, http://www.criver.com/) were bred and maintained in the animal facility at KU Leuven, Belgium. During the experiments, mice were maintained in isolator cages, fed with autoclaved acidified water, and irradiated food ad libitum. Animal procedures were performed according to protocols approved by the Institutional Ethics Committee.

2.2. Isolation of LT-HSC from bone marrow and fetal liver

Total adult bone marrow (ABM) cells were flushed from femurs and tibiae of male C57BL/6J mice, pooled, washed twice with phosphate-buffered saline (PBS; Gibco Invitrogen, CA) containing 0.1% bovine serum albumin (BSA; Sigma). Lineage negative cell isolation was performed using lineage cell depletion kit (Miltenyi Biotec, Germany). To isolate LT-HSCs from ABM, resulting Lin^- cells were stained with FITC conjugated anti-Sca-1, PE conjugated anti-c-kit, APC conjugated anti-lineage antibody cocktail (BD Pharmingen, San Diego, CA), PerCP/Cy5.5 conjugated anti-CD150 and APC conjugated anti-CD48 antibodies. Cells were incubated on ice for 30 min.

FL tissues were obtained from C57BL/6J embryos dissected at embryonic day (E) 14.5 (14 days after vaginal plug was observed). Ter-119 positive erythrocytes and erythrocyte progenitors were depleted using MACS columns (Miltenyi Biotec, Germany) and stained with Alexa Fluor 488 conjugated anti-lineage antibody cocktail (containing CD4, CD5, CD8a, CD45R, Ter-119, GR-1 antibodies), PE conjugated anti-CD11b, APC conjugated anti-Sca-1, PE-Cy7 conjugated anti-CD150 and Alexa Fluor 488 conjugated anti-CD48. Cells were incubated on ice for 30 min.

HSCs were sorted by fluorescence-activated cell sorting (FACS), using a FACS ARIAIII (Becton Dickinson).

2.3. RNA sequencing and bioinformatics analysis

To compare the gene expression between ABM and FL HSCs, total RNA was isolated from two biological replicates each of LT-HSCs from E14.5 FL and adult BM using miRNeasy Micro Kit (QIAGEN) and amplified with the Ovation RNA-seq V2 system (NuGen Technologies, CA) as per manufacturer's instructions. Amplified cDNA (1 μg) was sheared using the Covaris system (Covaris, MA) and fragments of 200 bp (180–220 bp) were selected to construct a cDNA library. The libraries were subjected to 2*90 bp paired-end sequencing on an Illumina HiSeq2000 sequencer. Raw reads generated by Illumina HiSeq2000 were subjected to quality control. Sequence reads were pre-processed by the pipeline of BGI (Shenzhen, China) to remove adaptors and filter low quality reads. The high quality reads were aligned to the mouse reference genome mm9 using TopHat2 tool (Kim et al. 2013).

The differential gene expression analysis was performed using the R package DESeq2 (Love et al. 2014) and differentially expressed genes were identified using the following thresholds: false discovery rate (FDR) < 0.05 and |log fold change| > 1.0. Gene-set enrichment analysis (GSEA) was performed to detect significantly enriched gene sets (also called pathways) using the R package GAGE v2.14.4 (Luo et al. 2009). The manually curated gene-set source was downloaded from the Bader lab (http://baderlab.org/GeneSets), which consisted of multiple data repositories, e.g. GO (Ashburner et al. 2000), Reactome (Croft et al. 2011), and Kyoto Encyclopedia of Genes and Genomes (KEGG) database (Ogata et al. 1999). GSEA results were visualized by Enrichment Map v2.1.0 (Merico et al. 2010) and Cytoscape v3.2.1 (Shannon et al. 2003). To further investigate differences on metabolic potential, KEGG metabolic pathway maps were reconstructed to provide an overview of gene expression profiling and molecular interactions within a single pathway by using the R package Pathview (Luo and Brouwer 2013). All sequencing data are deposited at the ArrayExpress database (http://www.ebi.ac.uk/arrayexpress) with accession number: E-MTAB-4034.

KEGG pathway analysis was also applied on the published datasets with accession number: GSE37000 (McKinney-Freeman et al. 2012), GSE55525 (Beerman et al. 2014) and E-MTAB-2262 (McKinney-Freeman et al. 2012; Beerman et al. 2014; Cabezas-Wallscheid et al. 2014). In brief, normalized (FRMA method) datasets with accession numbers GSE55525 and GSE37000 were downloaded from In silico DB (https://insilicodb.com) and data sets on HSCs, progenitor and cultured HSCs were analyzed for differentially regulated pathways using KEGG pathway analysis. Normalized read-count for RNA-seq data related to accession number E-MTAB-2262, was downloaded from the published dataset by Cabezas-Wallscheid et al. 2014 and KEGG pathway analysis was performed.

2.4. Quantitative RT-PCR

To confirm levels of expression of some of the genes, independent samples of BM and FL HSCs were sorted to perform qRT-PCR. RNA was isolated from the FACS sorted cells using the miRNeasy micro kit (Qiagen, Hilden, Germany). RNA was amplified and cDNA synthesized using the Ovation RNA-seq V2 system (NuGen Technologies, CA) as per manufacturer's instructions. qRT-PCR was performed using the Platinum SYBR Green qPCR SuperMix-UDG (Invitrogen). The PCR reactions were carried out on the ViiA7 Real-Time PCR System (Applied Biosystems). A list of primers used for the qRT-PCR can be found in Table 1. Gene expression for different transcripts was calculated relative to β-actin as a housekeeping gene.

Table 1
List of primers used to perform quantitative RT-PCR for analyzing expression of OxPhos related genes.

Gene name	Forward primer	Reverse primer
Idh2	GGACCTTATCAGGTTTGCAC	CAGGTTGCTCTTAATGGTGTC
Atp5o	TTCCACCATCATGAGTGTCCA	GACGGGTCAGTCTTGATCTC
Sdhd	CAGCATTTCTCCAGGACCAG	CCTTGGAACCAGAGTGGTG
Cox4i1	ATGGGAGTGTTGTGAAGAGTG	ATGCGGTACAACTGAACTTTCTC
Cox7b	GGGTGAATTTGCACCAAGGC	GCTTCGAACTTGGAGACGGC
Ndufc1	AAGTTCTATGTCCGGGAGCC	TTGTGTGTTTGGATGAGATAAATCC
Ndufb6	GAACATGGTCTTTAAGGCGTACC	GGGCTTCGAGCTAACAATGG
Gpx1	ACACCGAGATGAACGATCTGC	TCTTCATTCTTGCCATTCTCCTGG
Cat	ACAATGTCACTCAGGTGCGG	GCAATGTTCTCACACAGGCG
Prdx1	TATCAGATCCCAAGCGCACC	AAGGCCCCTGAAAGAGATACC

2.5. Mitochondria and cellular ROS level measurement

For both mitochondria and ROS staining, freshly isolated adult BM and E14.5 FL cells (2–3 × 10^6 cells/sample) were stained for 30 min at 4 °C with an anti-lineage antibody cocktail containing CD4, CD11b, CD5, CD8a, CD45R, Ter-119, Gr-1 (CD11b was excluded from FL samples), anti-Sca-1, anti-c-kit, anti-CD150 and anti-CD48 (anti-CD48 was included in lineage cocktail). For LSK cells from BM and FL, we stained for anti-lineage antibodies (cd11b was excluded from FL samples), anti-Sca-1 and anti-ckit. All the antibodies were conjugated with different fluorophores and were used in different color combination described in Table 1.

To measure mitochondrial mass, antibody labeled cells were incubated at 37 °C for 30 min in medium (IMDM with 10% FBS; Invitrogen) containing 100 nM MitoTracker Green FM (Invitrogen), and then analyzed with flow cytometry.

To measure cellular ROS levels, cells were cultured in IMDM supplemented with 10% FBS with or without Rotenone (15 μM, DMSO was used as vehicle control) for 90 min followed by PBS wash. Cells were then incubated with PBS containing 2 μM CM-H2DCFDA (Invitrogen) and with or without Rotenone at 37 °C for 30 min after being stained with the antibodies described in Table 2. ROS levels in the HSC gated population were quantified using flow cytometry.

To measure mitochondrial ROS levels, cells were cultured in IMDM supplemented with 10% FBS with or without Rotenone (15 μM; DMSO was used vehicle control) for 90 min followed by PBS wash. Cells were then incubated with PBS containing 5 μM MitoSox Red (Invitrogen) with/without Rotenone at 37 °C for 15 min after being stained with the antibodies described in Table 1. ROS levels in the HSC gated population were quantified using flow cytometry. All the samples were analyzed on a BD FACS Canto (BD Bioscience), except MitoSox Red staining, which was analyzed on a BD FACS AriaIII (BD Bioscience). All flow cytometry data were analyzed and quantified using the FlowJo software (Tree Star, San Carlos, CA, USA).

2.6. ATP measurement

ATP levels were quantified in FL and BM LT-HSC using the CellTiter-Glo Luminescent Cell Viability Assay Kit (Promega) according to manufacturer's protocol. In brief, FL and BM LT-HSC were FACS sorted (8000 cells per sample, n = 3) in IMDM basal medium (Invitrogen) and transferred to a 96-well opaque plate. Cells were equilibrated at room temperature (RT) for 30 min, subsequently substrate was added to each well and incubated for 10 min at RT. After, incubation luminescence was measured using the Victor3 plate reader (PerkinElmer, Inc.).

2.7. Oxygen consumption assay

The oxygen consumption rate (OCR) of LSK cells sorted from adult BM and E14.5 FL was measured using the XFp Extracellular Flux

Table 2
List of antibodies used in combination with fluorescent dyes for mitochondrial and ROS content analysis.

Dyes/experiment	Fluorophores	Antibodies	Clone	Company
MitoTracker Green FM/total mitochondrial content	PE	Anti-TER-119	Ter-119	BD
		Anti-Ly-6G/Ly-6C	RB6-8C5	BD
		Anti-CD4	GK1.5	ebioscience
		Anti-CD45R/B220	RA3-6B2	ebioscience
		Anti-CD8a	53-6.7	ebioscience
		Anti-CD5	53-7.3	BD
		Anti-CD48	HM48-1	BD
		Anti-cd11b	M1/70	ebioscience
	PerCP-Cy5.5	Anti-Sca-1	D7	ebioscience
	PE-Cy7	Anti-CD150	TC15-12F12.2	Biolegend
	APC	Anti-c-kit	2B8	ebioscience
MitoSox Red/mitochondrial ROS	AlexaFluor-488	Anti-TER-119	Ter-119	Biolegend
		Anti-Ly-6G/Ly-6C	RB6-8C5	Biolegend
		Anti-CD4	GK1.5	Biolegend
		Anti-CD45R/B220	RA3-6B2	Biolegend
		Anti-CD8a	53-6.7	Biolegend
		Anti-CD5	53-7.3	Biolegend
		Anti-CD48	HM48-1	Biolegend
	FITC	Anti-cd11b	M1/70	ebioscience
	APC	Anti-Sca-1	D7	ebioscience
	PE-Cy7	Anti-CD150	TC15-12F12.2	Biolegend
	APC-H7	Anti-c-kit	2B8	BD
CM-H2DCFDA/total ROS	PE	Anti-TER-119	Ter-119	BD
		Anti-Ly-6G/Ly-6C	RB6-8C5	BD
		Anti-CD4	GK1.5	ebioscience
		Anti-CD45R/B220	RA3-6B2	ebioscience
		Anti-CD8a	53-6.7	ebioscience
		Anti-CD5	53-7.3	BD
		Anti-CD48	HM48-1	BD
		Anti-cd11b	M1/70	ebioscience
	PerCP-Cy5.5	Anti-Sca-1	D7	ebioscience
	PE-cy7	Anti-CD150	TC15-12F12.2	Biolegend
	APC	Anti-c-kit	2B8	ebioscience

Analyzer (Seahorse Bioscience). For the measurement of the OCR, LSK cells (0.5–1 × 10^5) were FACS sorted from E14.5 FL and adult BM and plated in wells of the XFp plate coated with Cell-Tak adhesive, in 50 μl SFEM medium containing TPO (100 ng/ml) and SCF (50 ng/ml). The plates were centrifuged for 2 min at 200 × g (without acceleration/deceleration) to immobilize HSCs and incubated for 25 min at 37 °C. After the incubation period, additional 125 μl medium was added gently and plates were further incubated for 30 min. Seven basal respiration measurements were recorded followed by four measurements after oligomycin (ATP synthase inhibitor) treatment.

2.8. Statistical analysis

The significance of differences was determined by two-tailed Student's t-test. $p < 0.05$ was considered statistically significant (ns: not significant; *$p < 0.05$).

3. Results and discussion

3.1. Enrichment of OxPhos, TCA and DNA repair gene sets in FL versus BM derived LT-HSCs

For the RNA-seq study, we isolated LT-HSCs from E14.5 FL ($CD150^+$-$CD48^-Lin^-Sca\text{-}1^+CD11b^+$) and adult BM ($CD150^+CD48^-Lin^-Sca\text{-}1^+c\text{-}kit^+$) (Fig. 1A and Fig. S1A) by fluorescence activated cell sorting (FACS) and performed 90 bp pair-end RNA-seq. Raw sequencing reads filtered into clean reads, were aligned to the reference genome using the TopHat2 tool. On average, ≈88.0% of filtered reads per sample were mapped to the mouse genome (Fig. S1). Hierarchical clustering of E14.5 FL and BM LT-HSCs showed that both populations differ globally in gene expression profile, while biological replicates were highly correlated (Fig. S1C, D).

To determine which gene pathways are differentially expressed between FL and BM LT-HSCs, we performed a gene-set analysis

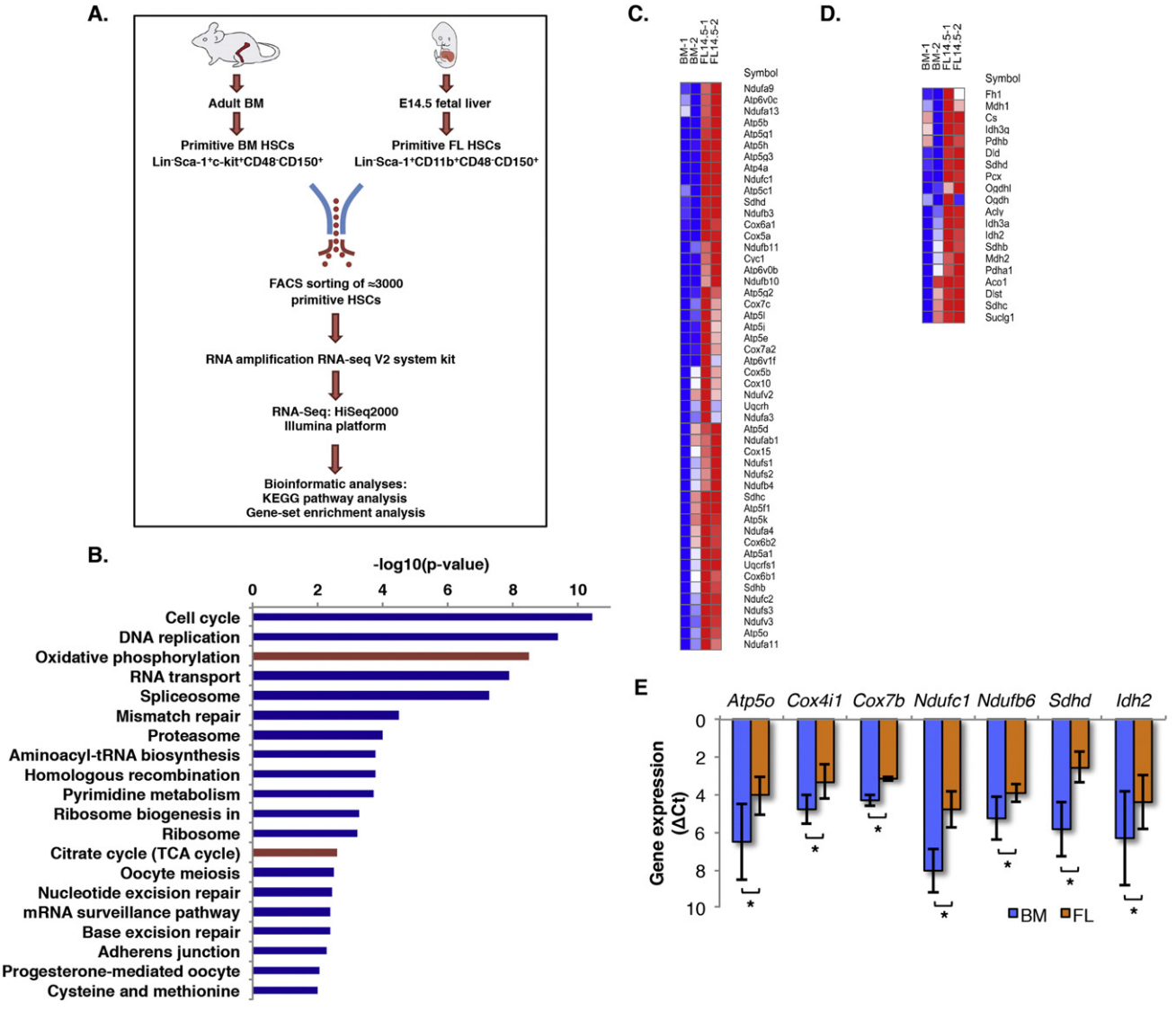

Fig. 1. Genes regulating oxidative phosphorylation are enriched in E14.5 FL derived LT-HSCs. A) Graphical presentation of the methods involved. Primitive HSCs FACS, sorted from adult BM and E14.5 FL, were subjected to RNASeq analysis. GSEA and KEGG pathway analysis was performed to assess pathway related gene clusters enriched in each sample. B) Pathways enriched in E14.5 FL LT-HSCs as compared with BM LT-HSCs identified by KEGG pathway analysis. For the top 20 up-regulated pathways, $\log_{10}$ for p-values were plotted and highlighted oxidative phosphorylation and TCA cycle pathways were in red. C, D) Heat map showing relative expression of the genes involved in oxidative phosphorylation (C) and TCA cycle (D) differentially regulated in FL versus BM derived LT-HSCs identified by KEGG pathway analysis. E) Increased expression of representative genes from oxidative phosphorylation and TCA cycle up regulated in FL LT-HSCs. ATP synthase subunit O (Atp5o), cytochrome c oxidase subunit 4 isoform 1 (Cox4i1) and subunit 7B (Cox7b), NADH dehydrogenase 1 subunit C1 (Ndufc1) and subunit B6 (Ndufb6), succinate dehydrogenase-D (Sdhd), isocitrate dehydrogenase (Idh2) were confirmed using qRT-PCR on at least three additionally isolated LT-HSC samples. For all samples ΔCt values for each gene were plotted. (n = 3–5, t test: *$p < 0.05$).

wherein functionally related gene-sets (designated pathways, hereafter) were grouped as network clusters (Fig. S1E). In total, 525 pathways (out of 8463) were significantly enriched in FL (480) and BM (45) HSCs (BM HSCs as control; p-value < 0.001 and FDR < 0.05). In addition, to identify differentially regulated pathways, we also performed KEGG pathway analysis (Fig. 1B). Cell cycle and DNA replication related gene sets were more highly expressed in FL LT-HSCs than in BM LT-HSCs, in line with differences in proliferation between FL and BM LT-HSCs. Extensive proliferation of adult BM LT-HSCs has been linked to the loss of stemness and DNA damage, resulting in premature aging (Mohrin et al. 2010). GSEA analysis showed higher expression of DNA repair pathway related genes in FL HSCs (Fig. S1E). Likewise, KEGG pathway analysis identified genes related to mismatch repair, homologous recombination, nucleotide and base excision repair pathways to be higher expressed in FL than BM LT-HSCs (Fig. 1B). This finding is in accordance with a recent study demonstrating that when brought into cell cycle, aged HSCs activate DNA damage responses (Beerman et al. 2014).

Interestingly, both GSEA (Fig. S1E) and KEGG pathway analysis (Fig. 1B) clearly showed that E14.5 FL LT-HSCs were enriched in gene-sets related to oxidative metabolic pathways such as OxPhos (Fig. 1C) and the TCA cycle (Fig. 1D). Increased expression of representative OxPhos and TCA cycle genes in FL LT-HSCs was confirmed by qRT-PCR (Fig. 1E). These findings are unexpected, as BM LT-HSCs, like many other adult stem cells, depend on glycolysis for energy production (Parmar et al. 2007), and inhibition of glycolytic pathways and activation of oxidative pathways correspond with lineage commitment of HSCs (Takubo et al. 2013). These observations are in line with KEGG pathway analysis of the transcriptome studies published by McKinney-Freeman et al., wherein we identified oxidative phosphorylation to be the top significantly up-regulated pathway in E14.5 FL HSC compared with BM LT-HSCs (McKinney-Freeman et al. 2012) (Fig. S2A), an observation that was not addressed in that study.

We also compared the expression of OxPhos and TCA genes between committed progenitors and LT-HSCs in either FL or BM. qRT-PCR demonstrated that most of the OxPhos and TCA genes analyzed were significantly higher expressed in BM LSK cells (i.e. a combination of ST-HSCs and multipotent progenitors (MPPs)), compared to BM LT-HSCs (Fig. S2B), while differences between FL LSK cells and FL LT-HSCs were less pronounced (Fig. S2C). These results are consistent with KEGG pathway analysis of data published by Beerman et al., In that study, higher levels of OxPhos and TCA pathway genes were also seen in

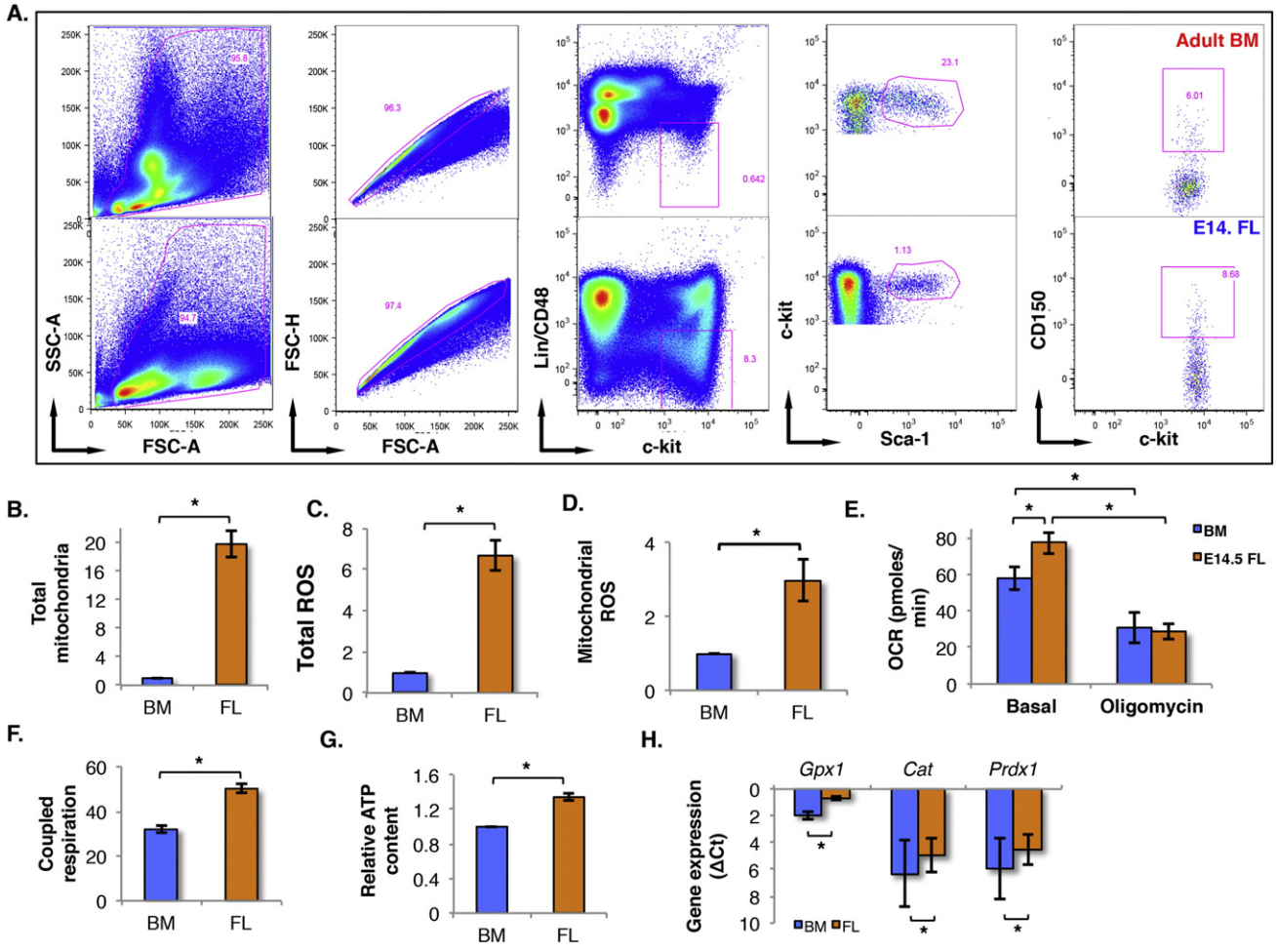

Fig. 2. Elevated levels of mitochondrial content and activity coupled with increased oxygen consumption in FL LT-HSCs. A) Mononuclear cells from adult BM (upper panel) and E14.5 FL (lower panel) were labeled with specific antibodies to identify primitive LT-HSCs (lower panel) and were co-stained with fluorescent dyes to quantify total mitochondrial content as well as total and mitochondrial ROS levels (plots are representative example of n = 3 biological replicates). B) Total mitochondrial content using MitoTracker Green FM dye was quantified in primitive LT-HSCs from BM and FL (n = 3, t test: *p < 0.05). C) ROS levels in BM and FL derived LT-HSCs were quantified using CM-H2DCFDA dye (n = 3, t test: *p < 0.05). D) Mitochondrial ROS levels in BM and FL LT-HSCs was quantified using MitoSox Red dye (n = 5 , t test: *p < 0.05). E) Oxygen consumption rate was measured in LSK cells isolated from FL (Orange) and BM (Blue) using the Seahorse Xp, in nine biological replicates, without and with addition of oligomycin (n = 9, t test: *p < 0.05). F) Coupled respiration was plotted for adult BM and E14.5 FL derived LSK cells (n = 9, t test: *p < 0.05). G) Quantification of ATP levels in FL LT-HSC relative to BM LT-HSC (n = 3, t test: *p < 0.05). H) Increased expression of representative genes from antioxidant pathways. Glutathione peroxidase 1 (*Gpx1*), Catalase (*Cat*) and Peroxiredoxin-1 (*Prdx-1*) up regulated in FL LT-HSCs were confirmed by qRT-PCR on at least three additionally isolated LT-HSC samples. For each gene ΔCt values representing the level gene expression were plotted for adult BM and E14.5 FL derived LT-HSCs (n = 3–5, t test: *p < 0.05).

MPP Flk2$^-$ progenitors compared with LT-HSCs, and TCA cycle genes were significantly higher expressed in MPP Flk2$^+$ progenitors (Fig. S2D–E) (Beerman et al. 2014). Moreover, granulocyte-macrophage progenitors were significantly more enriched for genes in the OxPhos, TCA cycle, and DNA damage response and repair pathways compared with LT-HSCs, and common lymphoid progenitors significantly enriched in OxPhos and DNA repair pathways (Fig. 2D–E). The same conclusions could be made from the study by Cabezas-Wallscheid et al., KEGG pathway analysis by pair-wise comparison of LT-HSCs with MPP1, MPP2, MPP3, MPP4 (i.e. different classes of multipotent progenitors) (Fig. S2D–E) demonstrated that MPPs are enriched for pathways related to cell-cycle, DNA-replication, mismatch repair, homologous recombination compared to HSC, and that, TCA cycle pathway genes were enriched in MPP2 and MPP3 compared with LT-HSCs (Fig. S2E) (Cabezas-Wallscheid et al. 2014).

Thus, compared with BM LT-HSCs, FL LT-HSCs express significantly higher levels of OxPhos and TCA genes as well as DNA repair genes, suggesting that FL LT-HSCs may be using oxidative phosphorylation to meet energy and building block needs. Once differentiated to more committed short-term (ST-) HSCs and MPPs, which can be seen as the transient amplifying pool of cells in hematopoiesis, expression of metabolic and DNA repair gene sets was significantly different from BM LT-HSC. However, in FL to perform more in depth comparison more difficult, as FL HSC sub-populations corresponding to the well-defined MMP, CMP and CLP subclassification have not been defined.

3.2. Higher mitochondrial content and oxygen consumption in FL derived LT-HSCs

Mitochondria are the sub-cellular sites of oxidative metabolic processes. The mitochondrial mass and activity in adult BM HSCs that depend upon glycolysis are low (Papa et al. 2012). By contrast, committed hematopoietic progenitors, which display higher oxidative phosphorylation and oxygen consumption levels, contain more and more active mitochondria compared with adult BM LT-HSCs (Romero-Moya et al. 2013). To demonstrate that the increased expression of OxPhos genes in FL LT-HSCs translates in the use of oxidative metabolic pathways, we first analyzed mitochondrial mass in primitive HSCs from E14.5 and adult BM (Fig. 2A, B). Mononuclear cells (MNCs) from 8-week-old murine BM and E14.5 murine FL were stained with antibodies against CD150, CD48, lineage markers, Sca-1 and c-kit (Fig. 2A), combined with mitochondrial dye. We used MitoTracker Green to examine the total mitochondrial content. Corroborating the increased expression of OxPhos genes in FL HSCs, we observed significantly higher total (Fig. 2B; Fig. S3A) mitochondrial content in FL than BM HSCs.

Mitochondrial staining also demonstrated that BM LSK cells had moderate but significantly higher mitochondrial content relative to BM LT-HSC (Fig. S3D–E). By contrast, the mitochondrial mass in FL LSK cells was modestly but significantly lower than in LT-HSC (Fig. S3F–G). Thus, compared to BM LT-HSC, BM LSK cells may have more active OxPhos metabolism. By contrast, minor differences in mitochondrial content were seen between FL-LSK cells and LT-HSC, suggesting that both populations use OxPhos metabolism, and more so than BM LT-HSC.

A number of studies demonstrated that production of reactive oxygen species (ROS), mainly the result of mitochondrial oxidation, induces HSC differentiation and aging, ultimately abrogating engraftment potential of adult BM HSCs (Ito et al. 2006). Hematopoietic stem and progenitor (HSPC; Lin$^-$CD45$^-$) cells containing low levels of ROS (ROS^{low}) were enriched in primitive HSC activity, while ROS^{hi} cells showed HSC exhaustion when serially transplanted (Jang and Sharkis 2007). We next analyzed total and mitochondrial ROS levels in FL and BM derived HSCs to assess if the greater mitochondrial mass in FL HSCs was associated with increased ROS production (Fig. 2C, D; Fig. S3B, C). Total cellular ROS content was assessed by staining primitive BM/FL MNCs with CM-H2DCFDA combined with HSC antibodies, while mitochondrial ROS, was assessed by staining MNCs with the MitoSox Red (mitochondrial superoxide–sensitive fluorophore) dye combined with HSC antibodies. We observed higher total (Fig. 2C; Fig. S3B) and mitochondrial (Fig. 2D; Fig. S3C) ROS levels in FL compared with adult BM LT-HSCs.

Finally, we measured the oxygen consumption rate (OCR) in FL and adult BM LT-HSCs. Due to the exceedingly low number of CD150$^+$-CD48$^-$Lin$^-$Sca-1$^+$c-kit$^+$ cell frequency in both adult BM and FL, we first tested if similar differences in mitochondrial content and activity observed in CD150$^+$CD48$^-$Lin$^-$Sca-1$^+$c-kit$^+$ BM vs. FL cells were also seen in the Lin$^-$Sca-1$^+$c-kit$^+$ (LSK) cell fraction. We found that differences in mitochondrial content between LSK cells from FL and BM were similar to what we found in the primitive HSC population (CD150$^+$CD48$^-$LSK cells) (data not shown). Therefore, we used LSK cells isolated form FL and adult BM for OCR studies using the Seahorse XFp analyzer. Basal respiration in FL LSK cells was significantly higher compared to BM LSK cells (Fig. 2E). Treatment of both FL and adult BM LSK cells with oligomycin, an inhibitor of the ATP synthase complex, significantly decreased OCR, demonstrating that the increased oxygen uptake in FL LT-HSCs was coupled with ATP generation via oxidative phosphorylation. This also showed that level of coupled respiration was significantly higher in E14.5 FL than in the adult BM LT-HSCs (Fig. 2F). Consistent with this OCR measurement, FL LT-HSCs showed significantly higher amount of cellular ATP levels relative to BM LT-HSCs due to higher OxPhos activity (Fig. 2G).

4. Conclusion

Our studies thus clearly demonstrate that FL LT-HSCs use OxPhos (aside from glycolysis), which we hypothesize is required to more efficiently generate ATPs and other building blocks essential for the extensive FL-HSC expansion. Unlike adult BM LT-HSCs, wherein OxPhos results in ROS accumulation causing differentiation, DNA damage and aging, LT-HSCs derived from FL that express higher levels of gene-sets related to “cellular response to stress” as well as DNA repair pathways may be able to cope with the increased ROS levels (Fig. 1B; Figs. S1E and S2A). Expression levels of some anti-oxidant genes from these gene-sets were examined in adult BM and E14.5 FL derived LT-HSCs by qRT-PCR (Fig. 2H). We speculate that elevated levels of these genes prevent DNA damage higher baseline ROS and oxygen consumption rate (OCR) in FL LT-HSCs (Nijnik et al. 2007; Rossi et al. 2007).

Thus, we here demonstrate, for the first time, that in contrast to adult BM LT-HSCs, FL LT-HSCs use OxPhos (aside from glycolysis), which may be required to more efficiently generate ATP and other building blocks essential for the extensive FL-HSC expansion. Proliferating FL LT-HSCs can prevent (geno)toxicity induced by ROS because they also express significantly more anti-oxidant pathway and DNA repair pathway genes. It is tempting to speculate that if mitochondrial biogenesis combined with strengthened antioxidant and DNA repair pathways could be induced in adult BM LT-HSCs, BM LT-HSC expansion might become possible.

Author contributions

The author contributions in this manuscript were as follows: J.M., performed the experiments, acquired the data and drafted the manuscript; Z.X., performed bioinformatic analysis and drafted the manuscript; D.B., performed some of the experiments; R.B., provided theoretical input, interpreted the data and reviewed the manuscript; A.V., G.E., T.V., S.S., N.V.G., provided technical help; A.P-M., S.M-F, G.C., and P.C., provided theoretical input and critically reviewed the manuscript; S.K. and C.M.V., were responsible for the conception of the study, data analysis and interpretation, and manuscript writing.

Supplementary data to this article can be found online at http://dx.doi.org/10.1016/j.scr.2015.11.001.

Acknowledgements

This work was supported by an FWO funding (G085111N), an FWO grant (1.2.665.11.N.00) to S Khurana, an FWO grant (G085111N10), Odysseus funding, CoE-SCIL, PF03, and GOA/11/012 funding from KU Leuven, and the Vanwayenberghe fund to CM Verfaillie. The work of P. Carmeliet is supported by long-term structural funding-Methusalem Funding by the Flemish Government. The authors wish to thank Pier Andree Pentilla and Rob Van Rossom for assistance with FACS sorting and analysis and Sarah Schouteden for technical support.

References

Abu Dawud, R., Schreiber, K., Schomburg, D., Adjaye, J., 2012. Human embryonic stem cells and embryonal carcinoma cells have overlapping and distinct metabolic signatures. PLoS One 7, e39896.

Ashburner, M., Ball, C.A., Blake, J.A., Botstein, D., Butler, H., Cherry, J.M., Davis, A.P., Dolinski, K., Dwight, S.S., Eppig, J.T., Harris, M.A., Hill, D.P., Issel-Tarver, L., Kasarskis, A., Lewis, S., Matese, J.C., Richardson, J.E., Ringwald, M., Rubin, G.M., Sherlock, G., 2000. Gene ontology: tool for the unification of biology. The Gene Ontology Consortium, Nat. Genet. 25, 25–29.

Beerman, I., Seita, J., Inlay, M.A., Weissman, I.L., Rossi, D.J., 2014. Quiescent hematopoietic stem cells accumulate DNA damage during aging that is repaired upon entry into cell cycle. Cell Stem Cell 15, 37–50.

Berg, J.M., Tymoczko, J.L., Stryer, L., 2007. Biochemistry. 6th edition. W. H. Freeman and Company, New York.

Bowie, M.B., Kent, D.G., Dykstra, B., McKnight, K.D., McCaffrey, L., Hoodless, P.A., Eaves, C.J., 2007. Identification of a new intrinsically timed developmental checkpoint that reprograms keSy hematopoietic stem cell properties. Proc. Natl. Acad. Sci. U. S. A. 104, 5878–5882.

Cabezas-Wallscheid, N., Klimmeck, D., Hansson, J., Lipka, D.B., Reyes, A., Wang, Q., Weichenhan, D., Lier, A., von Paleske, L., Renders, S., Wunsche, P., Zeisberger, P., Brocks, D., Gu, L., Herrmann, C., Haas, S., Essers, M.A., Brors, B., Eils, R., Huber, W., Milsom, M.D., Plass, C., Krijgsveld, J., Trumpp, A., 2014. Identification of regulatory networks in HSCs and their immediate progeny via integrated proteome, transcriptome, and DNA methylome analysis. Cell Stem Cell 15, 507–522.

Cheng, T., Rodrigues, N., Shen, H., Yang, Y., Dombkowski, D., Sykes, M., Scadden, D.T., 2000. Hematopoietic stem cell quiescence maintained by p21cip1/waf1. Science 287, 1804–1808.

Croft, D., O'Kelly, G., Wu, G., Haw, R., Gillespie, M., Matthews, L., Caudy, M., Garapati, P., Gopinath, G., Jassal, B., Jupe, S., Kalatskaya, I., Mahajan, S., May, B., Ndegwa, N., Schmidt, E., Shamovsky, V., Yung, C., Birney, E., Hermjakob, H., D'Eustachio, P., Stein, L., 2011. Reactome: a database of reactions, pathways and biological processes. Nucleic Acids Res. 39, D691–D697.

Foudi, A., Hochedlinger, K., Van Buren, D., Schindler, J.W., Jaenisch, R., Carey, V., Hock, H., 2009. Analysis of histone 2B-GFP retention reveals slowly cycling hematopoietic stem cells. Nat. Biotechnol. 27, 84–90.

Higuchi, Y., Zeng, H., Ogawa, M., 2003. CD38 expression by hematopoietic stem cells of newborn and juvenile mice. Leukemia 17, 171–174.

Ito, K., Hirao, A., Arai, F., Takubo, K., Matsuoka, S., Miyamoto, K., Ohmura, M., Naka, K., Hosokawa, K., Ikeda, Y., Suda, T., 2006. Reactive oxygen species act through p38 MAPK to limit the lifespan of hematopoietic stem cells. Nat. Med. 12, 446–451.

Jang, Y.Y., Sharkis, S.J., 2007. A low level of reactive oxygen species selects for primitive hematopoietic stem cells that may reside in the low-oxygenic niche. Blood 110, 3056–3063.

Kim, D., Pertea, G., Trapnell, C., Pimentel, H., Kelley, R., Salzberg, S.L., 2013. TopHat2: accurate alignment of transcriptomes in the presence of insertions, deletions and gene fusions. Genome Biol. 14, R36.

Klimmeck, D., Hansson, J., Raffel, S., Vakhrushev, S.Y., Trumpp, A., Krijgsveld, J., 2012. Proteomic cornerstones of hematopoietic stem cell differentiation: distinct signatures of multipotent progenitors and myeloid committed cells. Mol. Cell. Proteomics 11, 286–302.

Love, M.I., Huber, W., Anders, S., 2014. Moderated estimation of fold change and dispersion for RNA-seq data with DESeq2. Genome Biol. 15, 550.

Luo, W., Brouwer, C., 2013. Pathview: an R/bioconductor package for pathway-based data integration and visualization. Bioinformatics 29, 1830–1831.

Luo, W., Friedman, M.S., Shedden, K., Hankenson, K.D., Woolf, P.J., 2009. GAGE: generally applicable gene set enrichment for pathway analysis. BMC Bioinf. 10, 161.

Matés, J.M., Segura, J.A., Campos-Sandoval, J.A., Lobo, C., Alonso, L., Alonso, F.J., Márquez, J., 2009. Glutamine Homeostasis and Mitochondrial Dynamics. Int. J. Biochem. Cell Biol. 41, 2051–2061.

McKinney-Freeman, S., Cahan, P., Li, H., Lacadie, S.A., Huang, H.T., Curran, M., Loewer, S., Naveiras, O., Kathrein, K.L., Konantz, M., Langdon, E.M., Lengerke, C., Zon, L.I., Collins, J.J., Daley, G.Q., 2012. The transcriptional landscape of hematopoietic stem cell ontogeny. Cell Stem Cell 11, 701–714.

Merico, D., Isserlin, R., Stueker, O., Emili, A., Bader, G.D., 2010. Enrichment map: a network-based method for gene-set enrichment visualization and interpretation. PLoS One 5, e13984.

Mohrin, M., Bourke, E., Alexander, D., Warr, M.R., Barry-Holson, K., Le Beau, M.M., Morrison, C.G., Passegue, E., 2010. Hematopoietic stem cell quiescence promotes error-prone DNA repair and mutagenesis. Cell Stem Cell 7, 174–185.

Nijnik, A., Woodbine, L., Marchetti, C., Dawson, S., Lambe, T., Liu, C., Rodrigues, N.P., Crockford, T.L., Cabuy, E., Vindigni, A., Enver, T., Bell, J.I., Slijepcevic, P., Goodnow, C.C., Jeggo, P.A., Cornall, R.J., 2007. DNA repair is limiting for haematopoietic stem cells during ageing. Nature 447, 686–690.

Oburoglu, L., Tardito, S., Fritz, V., de Barros, S.C., Merida, P., Craveiro, M., Mamede, J., Cretenet, G., Mongellaz, C., An, X., Klysz, D., Touhami, J., Boyer-Clavel, M., Battini, J.L., Dardalhon, V., Zimmermann, V.S., Mohandas, N., Gottlieb, E., Sitbon, M., Kinet, S., Taylor, N., 2014. Glucose and glutamine metabolism regulate human hematopoietic stem cell lineage specification. Cell Stem Cell 15, 169–184.

Ogata, H., Goto, S., Sato, K., Fujibuchi, W., Bono, H., Kanehisa, M., 1999. KEGG: Kyoto encyclopedia of genes and genomes. Nucleic Acids Res. 27, 29–34.

Papa, S., Martino, P.L., Capitanio, G., Gaballo, A., De Rasmo, D., Signorile, A., Petruzzella, V., 2012. The oxidative phosphorylation system in mammalian mitochondria. Adv. Exp. Med. Biol. 942, 3–37.

Parmar, K., Mauch, P., Vergilio, J.A., Sackstein, R., Down, J.D., 2007. Distribution of hematopoietic stem cells in the bone marrow according to regional hypoxia. Proc. Natl. Acad. Sci. U. S. A. 104, 5431–5436.

Romero-Moya, D., Bueno, C., Montes, R., Navarro-Montero, O., Iborra, F.J., Lopez, L.C., Martin, M., Menendez, P., 2013. Cord blood-derived CD34 + hematopoietic cells with low mitochondrial mass are enriched in hematopoietic repopulating stem cell function. Haematologica 98, 1022–1029.

Rossi, D.J., Bryder, D., Seita, J., Nussenzweig, A., Hoeijmakers, J., Weissman, I.L., 2007. Deficiencies in DNA damage repair limit the function of haematopoietic stem cells with age. Nature 447, 725–729.

Shannon, P., Markiel, A., Ozier, O., Baliga, N.S., Wang, J.T., Ramage, D., Amin, N., Schwikowski, B., Ideker, T., 2003. Cytoscape: a software environment for integrated models of biomolecular interaction networks. Genome Res. 13, 2498–2504.

Suda, T., Takubo, K., Semenza, G.L., 2011. Metabolic regulation of hematopoietic stem cells in the hypoxic niche. Cell Stem Cell 9, 298–310.

Sudo, K., Ema, H., Morita, H., Nakauchi, H., 2000. Age-associated characteristics of murine hematopoietic stem cells. J. Exp. Med. 192, 1273–1280.

Takano, H., Ema, H., Sudo, K., Nakauchi, H., 2004. Asymmetric division and lineage commitment at the level of hematopoietic stem cells: inference from differentiation in daughter cell and granddaughter cell pairs. J. Exp. Med. 199, 295–302.

Takubo, K., Nagamatsu, G., Kobayashi, C.I., Nakamura-Ishizu, A., Kobayashi, H., Ikeda, E., Goda, N., Rahimi, Y., Johnson, R.S., Soga, T., Hirao, A., Suematsu, M., Suda, T., 2013. Regulation of glycolysis by Pdk functions as a metabolic checkpoint for cell cycle quiescence in hematopoietic stem cells. Cell Stem Cell 12, 49–61.

Varum, S., Rodrigues, A.S., Moura, M.B., Momcilovic, O., Easley, C.A.T., Ramalho-Santos, J., Van Houten, B., Schatten, G., 2011l. Energy metabolism in human pluripotent stem cells and their differentiated counterparts. PLoS One 6, e20914.

Vaziri, H., Dragowska, W., Allsopp, R.C., Thomas, T.E., Harley, C.B., Lansdorp, P.M., 1994. Evidence for a mitotic clock in human hematopoietic stem cells: loss of telomeric DNA with age. Proc. Natl. Acad. Sci. U. S. A. 91, 9857–9860.

Wang, Y.H., Israelsen, W.J., Lee, D., Yu, V.W., Jeanson, N.T., Clish, C.B., Cantley, L.C., Vander Heiden, M.G., Scadden, D.T., 2014. Cell-state-specific metabolic dependency in hematopoiesis and leukemogenesis. Cell 158, 1309–1323.

Wilson, A., Laurenti, E., Oser, G., van der Wath, R.C., Blanco-Bose, W., Jaworski, M., Offner, S., Dunant, C.F., Eshkind, L., Bockamp, E., Lio, P., Macdonald, H.R., Trumpp, A., 2008. Hematopoietic stem cells reversibly switch from dormancy to self-renewal during homeostasis and repair. Cell 135, 1118–1129.